communications materials

Article

https://doi.org/10.1038/s43246-024-00507-2

N-type molecular doping of a semicrystalline conjugated polymer through cation exchange

Yu Yamashita [1,2] ✉, Shinya Kohno[1], Elena Longhi[3], Samik Jhulki[3], Shohei Kumagai[1], Stephen Barlow[3,4], Seth R. Marder[3,4,5], Jun Takeya [1,2] & Shun Watanabe [1] ✉

Control of electrical doping is indispensable in any semiconductor device, and both efficient hole and electron doping are required for many devices. In organic semiconductors, however, electron doping has been essentially more problematic compared to hole doping because in general organic semiconductors have low electron affinities and require dopants with low ionization potentials that are often air-sensitive. Here, we adapt an efficient molecular doping method, so-called ion-exchange doping, to dope electrons in a polymeric semiconductor. We initially reduce the polymeric semiconductor using one electron transfer from molecular dopants, and then the ionized dopants in the resulting air-unstable films are replaced with secondary ions via cation exchange. Improved ambient stability and crystallinity of the doped polymeric semiconductors are achieved when a specific bulky molecular cation was chosen as the secondary ion, compared to conventional methods. The presented strategy can overcome the trade-off relationship between reducing capability and ambient stability in molecular dopants, and a wider selection of dopant ions will help to realize ambient-stable electron conductors.

Impurity doping of semiconductors is essential for most semiconductor devices, and the pn junction and complementary metal-oxide-semiconductor inverter are indispensable building blocks for devices manufactured today[1]. Likewise as in Si-based electronic devices, doping of organic semiconductors (OSCs) has been applied in various opto-electronic devices, such as organic light-emitting diodes[2,3], organic field-effect transistors[4–6], bipolar transistors[7], organic photovoltaics[8,9], and organic thermoelectric devices[10–13]. In inorganic semiconductors, control of charge polarity can be achieved in a straightforward way by an introduction of atomic dopants with different valences. On the other hand, doping of OSCs is achieved by an admixture of molecular reductants or oxidants into host π-conjugated molecules[14,15]. Although dopant molecules have a wide variety of size, conformation, and reactivity, candidate n-dopants (reductants) that achieve an efficient one-electron transfer and robust stability in material/device processing and under device operation conditions are rather limited to date. Efficient solid-state electron transfer requires that the reductant's ionization potential (IP) is smaller than the OSC's electron affinity (EA). Typical EAs of electron-transport OSCs range from less than 3.0 eV to ca. 4.0 eV, and thus strong reducing agents are required for electron doping (n-type doping) and electron-doped states are often sensitive to atmospheric oxygen and water.

A practical strategy to control the nature of ions in doped polymeric semiconductors has been demonstrated recently. Hole-doped polymeric semiconductors with various dopant anions have been explored by anion exchange and related doping methods[16–22]. The process of anion exchange doping is initiated by electron transfer reactions between semiconductors and oxidants, where the cationic semiconductors and oxidant-derived anions form intermediate donor-acceptor ion pairs. Then, an introduction of secondary anions can give rise to a spontaneous anion exchange in the polymeric semiconductors. The most important feature of ion-exchange doping is the ability to separate the two fundamental requirements in molecular dopants; the strength of redox reactivity and guarantee of charge neutrality by self-ionization. As a reducing agent for electron doping, for instance, cobaltocene ($CoCp_2$)[23] with reasonably low IP (4.1 eV in the solid

[1]Material Innovation Research Center (MIRC) and Department of Advanced Materials Science, Graduate School of Frontier Sciences, The University of Tokyo, 5-1-5 Kashiwanoha, Kashiwa, Chiba 277-8561, Japan. [2]Research Center for Materials Nanoarchitectonics (MANA), National Institute for Materials Science (NIMS), 1-1 Namiki, Tsukuba, Ibaraki 205-0044, Japan. [3]School of Chemistry and Biochemistry and Center for Organic Photonics and Electronics, Georgia Institute of Technology, Atlanta, GA 30332-0400, USA. [4]Renewable and Sustainable Energy Institute, University of Colorado Boulder, Boulder, CO 80309, USA. [5]Departments of Chemistry and of Chemical and Biological Engineering, University of Colorado, Boulder, CO 80309, USA. ✉e-mail: YAMASHITA.Yu@nims.go.jp; swatanabe@edu.k.u-tokyo.ac.jp

state)[24] has been known to results in efficient but air-unstable electron doping for n-type OSCs[25]. In particular, reversible electron transfer between $CoCp_2$ and n-type OSCs means equilibrium concentrations of air-sensitive and volatile neutral $CoCp_2$ remain in doped OSCs and can ultimately lead to dedoping through reaction with air and/or sublimation. If cation exchange is applicable to $CoCp_2$ doped OSCs, various stable and redox-inert molecular cations X^+ could be introduced to electron-doped polymers ($[OSC^{\bullet-}\ CoCp_2^+] \rightarrow [OSC^{\bullet-}\ X^+]$), while utilizing the moderately strong reducing nature of $CoCp_2$.

In this study, we developed a cation-exchange doping method that enables the electron doping of semicrystalline polymeric semiconductors with stable and redox-inert closed-shell cations. The doped thin films were evaluated by UV-Vis absorption spectroscopy, elemental analysis, photoelectron spectroscopy, and electrical conductivity measurements. Our experimental observations supported our model of cation-exchange doping, as shown in Fig. 1a. The semiconductor thin films electron-doped via our method showed ambient stability depending on the molecular cation species introduced during ion exchange. In our study, high ambient stability was observed when a conjugated polymer thin film was doped with the bulky 1,3-dimesitylimidazolium ($dMesIM^+$, Fig. 1b) cation. Interestingly, the π-stacking of the polymeric semiconductor was maintained upon doping only when $dMesIM^+$ was employed, while use of other cations disturbed the π-stacking. Cation exchange doping with a wide choice of dopant cations will help facilitate explorations of the structure-property relationships in electron-doped OSCs.

Results and discussion

Confirmation of cation-exchange doping

UV-Vis measurements were employed to evaluate the doping efficiency of our method in a widely studied polymeric semiconductor, poly[N,N'-bis(2-octyldodecyl)naphthalene-1,4,5,8-bis(dicarboximide)-2,6-diyl]-*alt*-5,5'-(2,2'-bithiophene) (P(NDI2OD-T2))[26]. P(NDI2OD-T2) thin films were spin-coated on glass substrates and then thermally annealed. The thin films were chemically doped by immersing them in a doping solution containing cobaltocene ($CoCp_2$) with or without salts of organic cations. All the fabrication processes were conducted in a N_2-purged glove box, and absorption measurements were conducted in ambient air without encapsulation. The absorption spectra of a pristine (undoped) P(NDI2OD-T2) thin film is shown in Fig. 1c, where the lowest energy absorption peak is ca. 704 nm. The spectrum of a thin film doped using a solution containing only $CoCp_2$ is nearly identical to that of the pristine film. Although the thin film showed color changes upon chemical doping in the glove box, its color returned to that of the undoped film upon air exposure. This behavior is ascribed to the dedoping of the once-electron-doped thin film upon air exposure owing to the instability of $CoCp_2$[23,25]. When a combination of $CoCp_2$ and tetrabutylammonium (TBA) chloride was employed, the features of electron-doped P(NDI2OD-T2)[25] were observed via the measurement in ambient air (Fig. 1d), indicating that unlike the $CoCp_2$-doped film, this thin film does not undergo rapid dedoping. Here, the intensity of the lowest energy excitation of pristine P(NDI2OD-T2) with a peak at 704 nm was decreased. At the same time, new features with peak at 496, 696, and 798 nm emerged. The peak observed in the pristine film at 392 nm moves to slightly shorter wavelength of 370 nm. All of these features agree with the changes in UV-Vis spectra observed during electrochemical doping of this polymer from neutral to radical anion state[27]. In this study, TBA^+ salts with PF_6^- and bis(trifluoromethanesulfonyl)imide ($TFSI^-$) were also employed (Fig. 1d). The observed ambient stability of the doped state indicates that the anionic charges in the doped polymer thin films are not compensated by $CoCp_2^+$ but rather by TBA^+ through the mechanism described in Fig. 1a. Note that these spectral changes were not observed when P(NDI2OD-T2) thin films were immersed in salt solutions without $CoCp_2$ (Supplementary Note 2), suggesting both salts and $CoCp_2$ play key roles. Improvements in the ambient stability of all the employed counter-anions imply that this phenomenon is not a anion-specific reaction but likely to be an ion-exchange reaction where anions simply serve as spectator ions. Combinations of $CoCp_2$ and the bulky organic cations of tetraphenylphosphonium (TPP^+) and $dMesIM^+$ were also tested; in this case, absorption spectra similar to those obtained with the TBA^+ salts were obtained (Fig. 1e). While a pristine

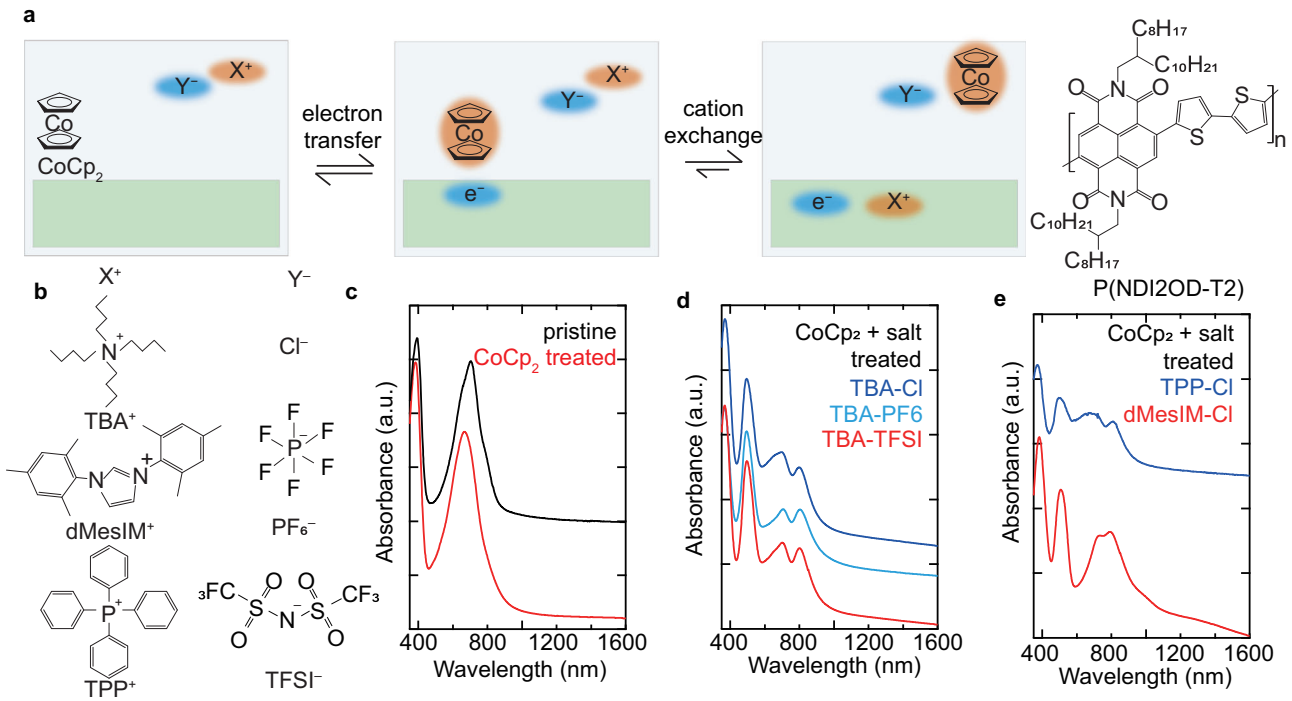

Fig. 1 | Cation-exchange doping. a Illustration of the cation-exchange doping process. **b** Chemical structures of the employed ionic compounds. **c** UV-Vis absorption spectra of pristine and $CoCp_2$-doped P(NDI2OD-T2) thin films. UV-Vis absorption spectra of P(NDI2OD-T2) thin films processed with combinations of (**d**) $CoCp_2$ and TBA^+ salts (**e**) $CoCp_2$ and TPP^+ or $dMesIM^+$ salts. UV-Vis spectra were all acquired in ambient air. The spectra are shown with offsets to improve the visibility.

P(NDI2OD-T2) thin film showed conductivity on the order of 10^{-8} S cm^{-1}, all the samples doped with combinations of $CoCp_2$ and salts showed conductivity on the order of 10^{-5} S cm^{-1} in air, which supports that the observed changes in UV-Vis spectra are ascribed to introduction of electrons in P(NDI2OD-T2) thin films. Detail of conductivity measurements and IV curves are available in Supplementary Note 3.

The identity of the dopant cations introduced into the P(NDI2OD-T2) thin films was further confirmed from the elemental composition revealed by X-ray photoelectron spectroscopy (XPS). Thin films of P(NDI2OD-T2) were prepared in the same manner as for the absorption measurements, except that the glass substrates were coated with Cr/Au prior to the fabrication of the polymer films. The undoped P(NDI2OD-T2) thin film shows peaks from C 1s, N 1s, O 1s, and S 2p which is in agreement with the chemical structure of P(NDI2OD-T2) (Fig. 2a–d) Please see Supplementary Notes 4 and 5 for detailed peak analysis and spectra in a wide energy range. For the $CoCp_2$-doped thin film, peaks assigned to Co 2p were also observed (Fig. 2e). When $CoCp_2$ and dMesIM-Cl were employed in the chemical doping process, the peak intensity of Co 2p normalized by that of C 1s decreased by c.a. 87% compared with that of the $CoCp_2$-doped sample. In the N 1s region, peaks from different binding energies are overlapping, which was deconvoluted to nitrogen atoms in P(NDI2OD-T2) (399.71 ± 0.02 eV) and dMesIM$^+$ (401.63 ± 0.01 eV). The binding energy of the latter matches well with a literature value for a imidazolium structure[28]. Quantitative analysis suggests that the molar ratio of dMesIM$^+$/P(NDI2OD-T2) monomer was 0.85, suggestive of a high doping level at least near the surface of the film, assuming a homogeneous distribution of dopant ions. Please see Supplementary Note 4 for detail of deconvolution procedures. These observations suggest that the majority of $CoCp_2$ and its cationic form are replaced by dMesIM$^+$ during doping. When $CoCp_2$ and TPP-Cl were employed for chemical doping, the peak intensity of Co 2p became comparable with that of the dMesIM$^+$-doped sample. A clear P 2p peak was observed, indicating that TPP$^+$ is present in this thin film (Fig. 2f). The molar ratio of TPP$^+$/P(NDI2OD-T2) monomer was estimated to be 1.10. Overall, the absorption, conductivity and XPS measurements support the supposition that cation exchange occurs in our chemical doping method, in which P(NDI2OD-T2) thin films are mainly doped with bulky organic cations such as TPP$^+$ and dMesIM$^+$.

The IP values of the cation-exchange-doped thin films were evaluated using photoelectron yield spectroscopy (PYS). In this method, photoelectron yield was obtained while sweeping the wavelength of incident UV light. In the analysis of the PYS measurements, the cube root of the photoelectron yield was plotted, the threshold of which showed the IP values of the organic materials[29]. The IP of the undoped P(NDI2OD-T2) originates from the highest occupied molecular orbital (HOMO) of the polymer, which is evaluated to be 5.8 eV and close to the reported value[30] (Fig. 3a). When this polymer is heavily electron-doped, a large decrease in IP is expected because of the filling of the lowest unoccupied molecular orbital (LUMO) with electrons. Such large shifts in IP were observed for the TPP$^+$- and dMesIM$^+$-doped thin films (Fig. 3b). The resulting IP is comparable with the known LUMO level of this polymer[30], which supports the successful electron doping of the LUMO of P(NDI2OD-T2).

Ambient stability

The effects of the dopant cations on the stability of the doped P(NDI2OD-T2) thin films were evaluated using UV-Vis measurements. Based on the measured IP values, the electron-doped P(NDI2OD-T2) thin films are expected to be dedoped under ambient conditions owing to their redox reactions with water and oxygen[2]. In this study, dimeric dopants that showed moderate ambient stability before and after chemical doping[25,31] were also tested as a comparison. Dimers of 2-(4-dimethylaminophenyl)-

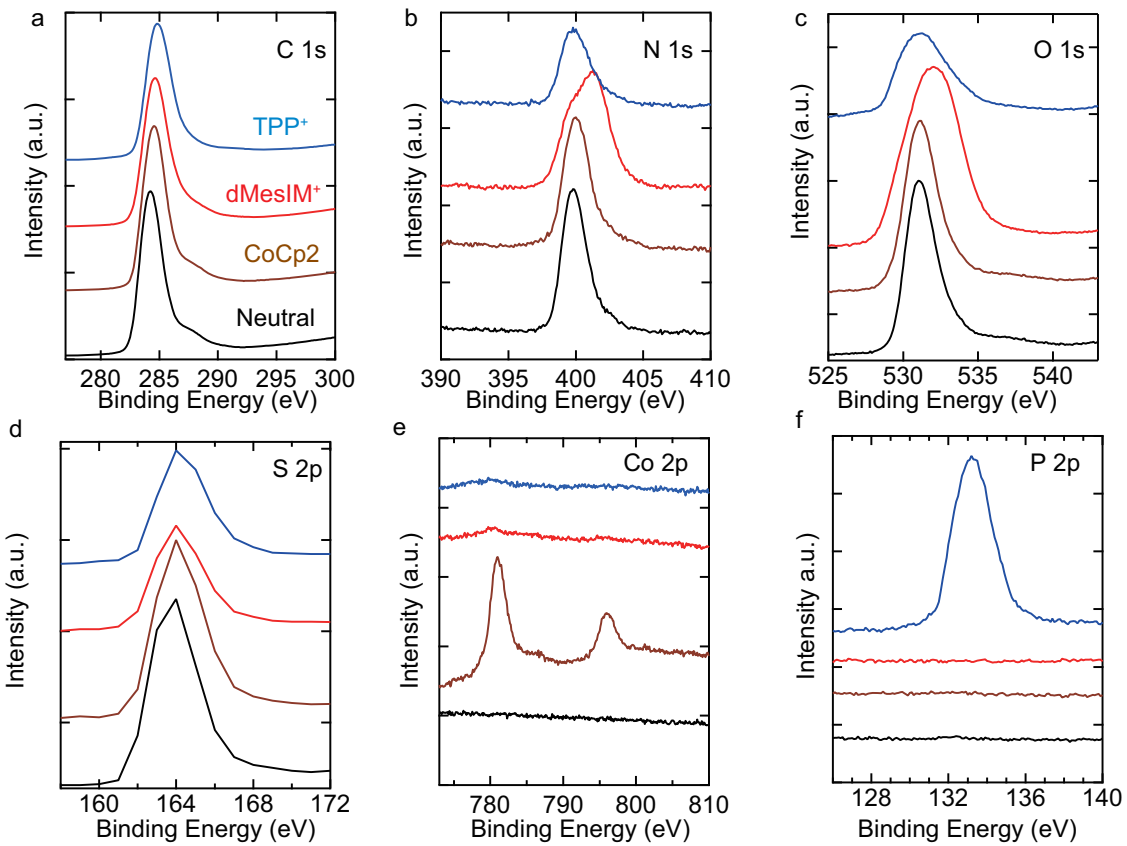

Fig. 2 | Elemental analysis of the electron-doped conjugated polymers. XPS signals obtained from the pristine, $CoCp_2$-doped, and cation-exchange-doped P(NDI2OD-T2) thin films. The names of the cation species are denoted for the cation-exchange-doped samples. The signals of the peak positions for (**a**) C 1s, (**b**) N 1s, (**c**) O 1s, (**d**) S 2p, (**e**) Co 2p, and (**f**) P 2p are shown.

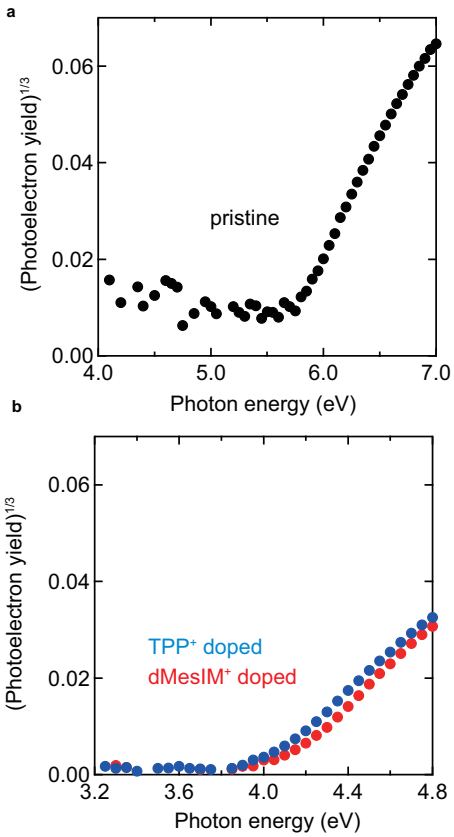

Fig. 3 | Photoelectron yield spectroscopy measurements of the electron-doped conjugated polymers. Plots of the photoelectron yields obtained from the (**a**) pristine and (**b**) cation-exchange-doped P(NDI2OD-T2) thin films. The names of the cation species are denoted for the cation-exchange-doped samples.

1,3-dimethylbenzo[*d*]imidazole (N-DMBI) and RuCp*Mes (Cp* = pentamethylcyclopentadienyl; Mes = 1,3,5-trimethylbenzene) were dissolved in a doping solution without salts. In this case, N-DMBI$^+$ and RuCp*Mes$^+$ are the dopant cations for the electron-doped P(NDI2OD-T2). The absorption spectra of the processed thin films measured under ambient conditions showed the features of electron doping consistent with the literature[27], demonstrating the superior ambient stability of these dopants compared with $CoCp_2$ (Fig. 4a, b). However, in our stability tests, the thin films doped with these dopants showed dedoping upon exposure to humid air of 20 °C and 80% relative humidity for 1 h. Dedoping was suggested also for thin films doped with TBA$^+$ or TPP$^+$ through cation exchange in the stability test (Fig. 4c, d). By contrast, the thin film doped with dMesIM$^+$ exhibited improved stability in humid air. The ratio of doped fraction in a thin film, θ, was evaluated for the dMesIM$^+$-doped sample based on the UV-Vis spectra (Fig. 4f). θ was defined to be unity at 0 h in the durability test and calculated based on the relative area of the peak at 509 nm that appears in doped samples. Please see Supplementary Note 6 for detail. Conductivity also showed prolonged lifetime when using this dopant (Supplementary Fig. S2).

The ambient stability of OSCs doped with redox-inert closed-shell ions has recently been discussed, and the effects of the ion size[16,18] and supramolecular structures[32,33] of semiconductor-dopant pairs have been reported. Given the ion-size effect and calculated volumes of dopant cations (Table 1), it is unclear why the dMesIM$^+$-doped thin film shows higher stability than the films doped with other dopant cations. One possibility is that the crystalline structure of the film affects the stability of the doped state[32,33], as discussed below.

Thin-film structures

The crystalline structures of the electron-doped P(NDI2OD-T2) thin films were evaluated through X-ray scattering measurements (Fig. 5a–f), which proved that the dopant cation species had considerable effects on the structures. Pristine P(NDI2OD-T2) show the features of face-on orientations[34] (Fig. 5a). The (*h*00) diffraction peaks originating from the

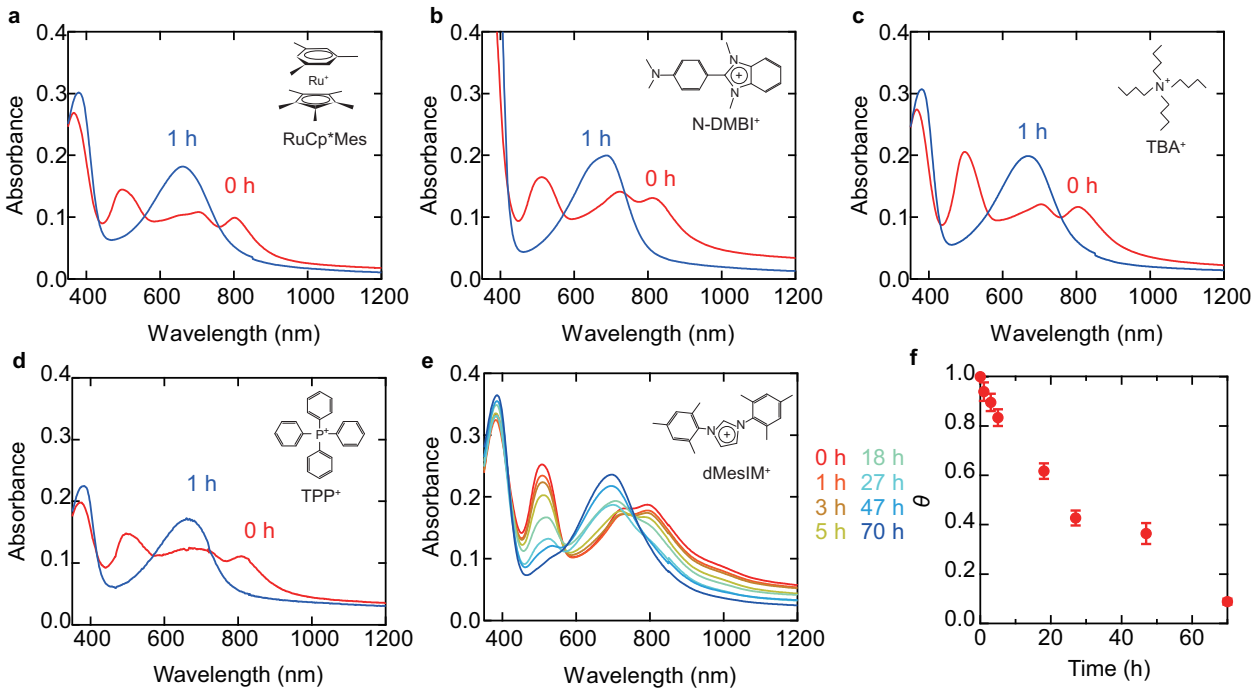

Fig. 4 | Stability of the electron-doped polymer thin films under humid conditions. UV-vis spectra of doped P(NDI2OD-T2) thin films before and after exposure to humidity conditions of 20 °C and 80% RH. Doping with (**a**) $(RuCp^*Mes)_2$, (**b**) $(N\text{-}DMBI)_2$, (**c**) TBA$^+$ exchange, (**d**) TPP$^+$ exchange, and (**e**) dMesIM$^+$ exchange were employed. **f** Doping level θ estimated for dMesIM$^+$-doped thin film.

lamellar structures were observed mainly in the in-plane direction, whereas the (010) peak originating from π-stacking appeared in the out-of-plane direction (Fig. 5g–j). To evaluate changes in thin-film structures upon chemical doping, the (100) peak intensity observed in the in-plane direction $I_{(100)IP}$, out-of-plane direction $I_{(100)OP}$, and their sum $I_{(100)total}$ were estimated (See Supplementary Note 7 for fittings). Table 2 shows the ratio of the out-of-plane peak intensity to the total one, $I_{(100)OP}/I_{(100)total}$. TPP^+-doped film did not show clear diffraction peaks, which suggests disordered structure for this sample. TBA^+-, N-$DMBI^+$-, and RuCp*Mes^+-doped films showed values close to unity, suggesting greater fractions of the films were edge-on orientated or the crystallinities of the edge-on oriented fractions were higher compared to the pristine film. Note that in spin-coated films with randomly oriented polymer main chains, only small fractions of polymers with a specific angle to the incident x-ray can contribute to the in-plane direction diffraction peak, which decreases the intensity of in-plane to out-of-plane diffraction. This explains $I_{(100)OP}/I_{(100)total}$ of 0.53 for the pristine film, which has been reported to be face-on oriented[34]. In the in-plane direction, a clear peak at 0.9 $Å^{-1}$ was observed for RuCp*Mes^+-doped film (Fig. 5j); this peak is assigned to order along the main chain direction, i.e. to a (001') reflection[34,35]. This feature is consistent with a semicrystalline edge-on oriented character for the RuCp*Mes^+-doped film.

The $dMesIM^+$-doped thin film exhibited a relatively small value for $I_{(100)OP}/I_{(100)total}$ compared to other dopants. In addition to this, (010)π-stacking peak at 1.6 $Å^{-1}$ in the out-of-plane direction was maintained for this dopant but was not observed for the other dopants around this position (Fig. 5h). This feature was not observed when other imidazolium-based cations were used (Supplementary Note 8). The clear difference in crystalline structures with different dopants suggests that the choice of cation species has an impact on the crystalline structure, which affects the transport properties and ambient stability of the doped states. Face-on oriented, π-stacked structures in the $dMesIM^+$-doped thin film could contribute to the improved ambient stability observed in our study.

Table 1 | Volumes of dopant cation molecules

Name	Volume (nm^3)
TBA^+	0.39
$dMesIM^+$	0.38
N-$DMBI^+$	0.38
RuCp*Mes^+	0.33
TPP^+	0.46

Gaussian 16 was employed to optimize structures and calculate volumes. Molecular structures were optimized via DFT calculations based on the B3LYP functional and 6-31+G(d) basis set. The Lanl2DZ basis set was employed for RuCp*Mes^+, which includes a Ru atom.

Conclusion

In this study, we developed the cation-exchange doping method for polymeric semiconductors. Successful cation exchange from $CoCp_2$ to stable and redox-inert closed-shell cations was confirmed by absorption and XPS elemental analyses. The electron doping of the P(NDI2OD-T2) thin films was also confirmed by PYS measurements, where large shifts in IP were observed owing to the filling of the density of states in the LUMO of P(NDI2OD-T2). Durability under humid conditions was dramatically improved by employing $dMesIM^+$ in our method. The observed durability may be affected by the crystalline structures of the doped thin films. X-Ray scattering measurements showed that the cation species exerts considerable effects on the crystallinity and orientation of the

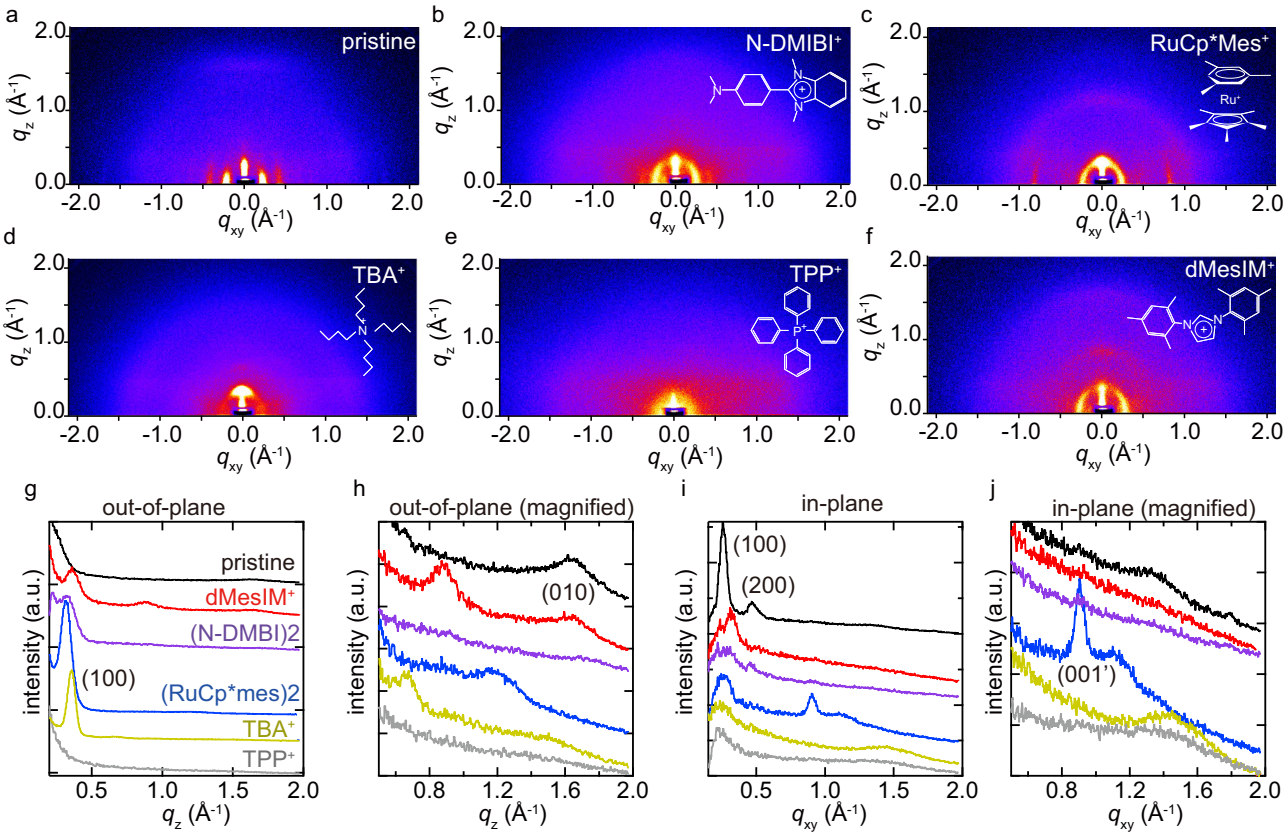

Fig. 5 | X-Ray scattering measurements of P(NDI2OD-T2) thin films doped with various dopants. X-Ray scattering images of P(NDI2OD-T2) thin films (**a**) in pristine state and after doping with (**b**) $(N\text{-}DMBI)_2$, (**c**) $(RuCp^*Mes)_2$, (**d**) TBA^+ exchange, (**e**) TPP^+ exchange, (**f**) and $dMesIM^+$ exchange. **g**, **h** Plots of intensities and their magnified versions for the out-of-plane and (**i**, **j**) the in-plane directions.

Table 2 | Ratio of (100) diffraction peaks observed in the in-plane and out-of-plane directions

Dopant	$I_{(100)OP}/I_{(100)total}$
Pristine	0.53 ± 0.13
N-DMBI$^+$	0.929 ± 0.009
RuCp*Mes$^+$	0.967 ± 0.003
TBA$^+$	0.938 ± 0.006
TPP$^+$	–
dMesIM$^+$	0.74 ± 0.02

electron-doped thin films. Our method presents new opportunities for future research on the structure-property relationships in doped materials with various dopant cations and the development of high-performance electron-doped OSCs.

Methods

Thin-film fabrication

High-purity glass substrates were employed for the optical and electrical measurements. Glass or Si substrates with naturally oxidized layers were employed for the X-ray scattering measurements. Glass substrates coated with Cr/Au electrodes were used for the XPS and PYS measurements. P(NDI2OD-T2) thin films were deposited via spin-coating. The resulting films were annealed on a hotplate at 180 °C for 30 min and then slowly cooled. The thickness of the films was determined to be 70 ± 5 nm using a Dektak surface profilometer. The P(NDI2OD-T2) thin films were doped by immersion in the dopant solutions for 5 min in an N_2-purged glove box. Detailed descriptions of the film preparation and doping procedures are presented in the Supplementary Note 1.

Thin-film evaluations

UV-Vis absorption spectra were obtained in air using a V-670 (JASCO) spectrometer. Electrical conductivities were measured in air using a Keithley 2612B source meter. XPS measurements were performed using a KRATOS ULTRA 2 instrument with monochromatic Al Kα X-rays. PYS spectra were obtained with a SUMITOMO PYS-202 system under vacuum using a turbomolecular pump system; here, a deuterium lamp (xenon lamp) was employed for the pristine (doped) thin films. 2D X-Ray scattering images were obtained using a RIGAKU SmartLab instrument with a MicroMax-007HF X-ray generator employing Cu Kα radiation ($\lambda = 0.15418$ nm).

DFT calculations

Structural optimization and evaluation of the molar volumes of the molecular ions were conducted using Gaussian 16 software. The B3LYP functional and 6-31+G(d) basis set were employed. The Lanl2DZ basis set was employed for RuCp*Mes$^+$, which includes a Ru atom.

Data availability

The data supporting the plots within this study are available from Zenodo at https://doi.org/10.5281/zenodo.10911316.

Received: 24 October 2023; Accepted: 16 April 2024;
Published online: 21 May 2024

References

1. Sze, S. M. *Semiconductor Devices: Physics and Technology* (John wiley & sons, 2008).
2. Tang, C. G. et al. Doped polymer semiconductors with ultrahigh and ultralow work functions for ohmic contacts. *Nature* **539**, 536 (2016).
3. Lin, X. et al. Beating the thermodynamic limit with photo-activation of n-doping in organic semiconductors. *Nat. Mater.* **16**, 1209–1215 (2017).
4. Kim, Y. et al. Enhanced Charge Injection Properties of Organic Field-Effect Transistor by Molecular Implantation Doping. *Adv. Mater.* **31**, 1806697 (2019).
5. Lussem, B. et al. Doped organic transistors. *Chem. Rev.* **116**, 13714–13751 (2016).
6. Kim, Y. et al. Highly Stable Contact Doping in Organic Field Effect Transistors by Dopant-Blockade Method. *Adv. Funct. Mater.* **30**, 2000058 (2020).
7. Wang, S.-J. et al. Organic bipolar transistors. *Nature* **606**, 700–705 (2022).
8. Lin, Y. et al. 17.1% efficient single-junction organic solar cells enabled by n-type doping of the bulk-heterojunction. *Adv. Sci.* **7**, 1903419 (2020).
9. Lin, Y. et al. A Simple n-Dopant Derived from Diquat Boosts the Efficiency of Organic Solar Cells to 18.3%. *ACS Energy Lett.* **5**, 3663–3671 (2020).
10. Russ, B., Glaudell, A., Urban, J. J., Chabinyc, M. L. & Segalman, R. A. Organic thermoelectric materials for energy harvesting and temperature control. *Nat. Rev. Mater.* **1**, 1–14 (2016).
11. Un, H.-I. et al. Understanding the effects of molecular dopant on n-type organic thermoelectric properties. *Adv. Energy Mater.* **9**, 1900817 (2019).
12. Patel, S. N. et al. Morphology controls the thermoelectric power factor of a doped semiconducting polymer. *Sci. Adv.* **3**, e1700434 (2017).
13. Kroon, R. et al. Bulk Doping of Millimeter-Thick Conjugated Polymer Foams for Plastic Thermoelectrics. *Adv. Funct. Mater.* **27**, 1704183 (2017).
14. Lüssem, B., Riede, M. & Leo, K. Doping of organic semiconductors. *Phys. Status Solidi A* **210**, 9–43 (2013).
15. Jacobs, I. E. & Moulé, A. J. Controlling molecular doping in organic semiconductors. *Adv. Mater.* **29**, 1703063 (2017).
16. Yamashita, Y. et al. Efficient molecular doping of polymeric semiconductors driven by anion exchange. *Nature* **572**, 634–638 (2019).
17. Ishii, M., Yamashita, Y., Watanabe, S., Ariga, K. & Takeya, J. Doping of molecular semiconductors through proton-coupled electron transfer. *Nature* **622**, 285–291 (2023).
18. Thomas, E. M. et al. Effects of counter-ion size on delocalization of carriers and stability of doped semiconducting polymers. *Adv. Electron. Mater.* **6**, 2000595 (2020).
19. Jacobs, I. E. et al. High-efficiency ion-exchange doping of conducting polymers. *Adv. Mater.* **34**, 2102988 (2022).
20. Murrey, T. L. et al. Anion Exchange Doping: Tuning Equilibrium to Increase Doping Efficiency in Semiconducting Polymers. *J. Phys. Chem. Lett.* **12**, 1284–1289 (2021).
21. Yuan, D. et al. Double Doping of Semiconducting Polymers Using Ion-Exchange with a Dianion. *Adv. Funct. Mater.* **33**, 2300934 (2023).
22. Jha, M. et al. Stability Study of Molecularly Doped Semiconducting Polymers. *J. Phys. Chem. C.* **128**, 1258–1266 (2024).
23. Connelly, N. G. & Geiger, W. E. Chemical redox agents for organometallic chemistry. *Chem. Rev.* **96**, 877–910 (1996).
24. Chan, C. K. et al. N-type doping of an electron-transport material by controlled gas-phase incorporation of cobaltocene. *Chem. Phys. Lett.* **431**, 67–71 (2006).
25. Yamashita, Y. et al. Highly air-stable, n-doped conjugated polymers achieved by dimeric organometallic dopants. *J. Mater. Chem. C.* **9**, 4105–4111 (2021).
26. Anthony, J. E., Facchetti, A., Heeney, M., Marder, S. R. & Zhan, X. n-type organic semiconductors in organic electronics. *Adv. Mater.* **22**, 3876–3892 (2010).
27. Trefz, D. et al. Electrochemical investigations of the n-type semiconducting polymer p (ndi2od-t2) and its monomer: New insights in the reduction behavior. *J. Phys. Chem. C.* **119**, 22760–22771 (2015).
28. Caporali, S., Bardi, U. & Lavacchi, A. X-ray photoelectron spectroscopy and low energy ion scattering studies on 1-buthyl-3-methyl-imidazolium bis (trifluoromethane) sulfonimide. *J. Electron Spectrosc. Relat. Phenom.* **151**, 4–8 (2006).
29. Ishii, H., Kinjo, H., Sato, T., Machida, S.-i. & Nakayama, Y. Photoelectron yield spectroscopy for organic materials and

interfaces. In *Electronic Processes in Organic Electronics*, 131–155 (Springer, 2015).
30. Qi, Y. et al. Solution doping of organic semiconductors using air-stable n-dopants. *Appl. Phys. Lett.* **100**, 54 (2012).
31. Mohapatra, S. K., Marder, S. R. & Barlow, S. Organometallic and organic dimers: Moderately air-stable, yet highly reducing, n-dopants. *Acc. Chem. Res.* **55**, 319–332 (2022).
32. Yamashita, Y. et al. Supramolecular cocrystals built through redox-triggered ion intercalation in π-conjugated polymers. *Commun. Mater.* **2**, 1–9 (2021).
33. Kurosawa, T. et al. Strong and atmospherically stable dicationic oxidative dopant. *Adv. Sci.* **8**, 2101998 (2021).
34. Rivnay, J. et al. Unconventional face-on texture and exceptional in-plane order of a high mobility n-type polymer. *Adv. Mater.* **22**, 4359–4363 (2010).
35. Rivnay, J. et al. Drastic control of texture in a high performance n-type polymeric semiconductor and implications for charge transport. *Macromolecules* **44**, 5246–5255 (2011).

Acknowledgements

This study was supported by JSPS KAKENHI (JP22H02160) and JST CREST Grant Number JPMJCR21O3. The synthesis of $(RuCp^*Mes)_2$ and $(N\text{-}DMBI)_2$ at Georgia Tech was supported by the National Science Foundation (through DMR-1807797/ 2216857, and through the DMREF program, DMR-1729737). Contributions to discussion of results and editing of the manuscript by S.B. and S.R.M. were supported by the Center for Soft PhotoElectroChemical Systems (SPECS), an Energy Frontier Research Center funded by the U.S. Department of Energy, Office of Science, Basic Energy Sciences under award No. DE-SC0023411.

Author contributions

Y.Y., S.W., S.B. and S.R.M. conceived the proof-of-concept of the doping method. Y.Y., S.Kohno, and S.Kumagai designed and performed the experiments and analyzed the data. E.L. and S.J. synthesized the $(RuCp^*Mes)_2$ and N-DMBI dimers. Y.Y. wrote the manuscript. S.B., S.R.M., S.W. and J.T. supervised the work. All authors discussed the results and reviewed the manuscript.

Competing interests

S.W. is an Editorial Board Member for Communications Materials and was not involved in the editorial review, or the decision to publish, this Article. The all other authors declare no competing interests.

Additional information

Supplementary information The online version contains supplementary material available at https://doi.org/10.1038/s43246-024-00507-2.

Correspondence and requests for materials should be addressed to Yu Yamashita or Shun Watanabe.

Peer review information *Communications Materials* thanks Ian Jacobs and the other, anonymous, reviewer(s) for their contribution to the peer review of this work. Primary Handling Editors: Jet-Sing Lee.